Atomic-Scale Photon Mapping Revealing Spin-Current Relaxation

Shunji Yamamoto, Hiroshi Imada, and Yousoo Kim

Phys. Rev. Lett. **128**, 206804 — Published 20 May 2022

DOI: 10.1103/PhysRevLett.128.206804

Atomic-scale photon mapping revealing spin-current relaxation

Shunji Yamamoto, Hiroshi Imada & Yousoo Kim*†

Surface and Interface Science Laboratory, RIKEN, Wako, Saitama 351-0198, Japan.

Abstract

A nanoscopic understanding of spin-current dynamics is crucial for controlling the spin transport in materials. However, gaining access to spin-current dynamics at an atomic scale is challenging. Therefore, we developed spin-polarized scanning tunneling luminescence spectroscopy (SP-STLS) to visualize the spin relaxation strength depending on spin injection positions. Atomically resolved SP-STLS mapping of gallium arsenide demonstrated a stronger spin relaxation in gallium atomic rows. Hence, SP-STLS paves the way for visualizing spin current with single-atom precision.

* Corresponding author.
† E-mail: ykim@riken.jp

The sub-nanoscale visualization of spin-current dynamics is crucial in gaining a fundamental understanding of spin transport phenomena [1,2]. Previous studies on spin-current dynamics in nanofabricated devices have revealed essential functionalities, including reading, writing, and transferring of spin information [3], many of which indicate the significant influence of local environments via spin-orbit coupling [1,3,4]. Spin-polarized scanning tunneling microscopy (SP-STM) [5,6], an experimental platform for atomic-scale spin injection and detection, enables the selective investigation of local spin behavior at the sample surfaces. The positional controllability of SP-STM has prompted its use in studies on local spin dynamics in atomic-scale impurities and adsorbates [7–9]. However, SP-STM employs tunnel magnetoresistance for imaging localized spins at the sample surface; hence, it would be desirable to provide additional access to diffusive spins and direct insights into spin current at an atomic scale.

Combining SP-STM with scanning tunneling luminescence spectroscopy (STLS) [10] offers a promising way to capture the diffusive spin current. Because luminescence in STLS occurs after electron injection followed by relaxation dynamics, luminescence spectroscopy facilitates the investigation of diffusive electron dynamics in materials. STLS studies have revealed various electron dynamical processes in local electronic states, such as surface states [11], molecules [12–14], and low-dimensional materials [15,16]. Therefore, the development of spin-polarized STLS (SP-STLS) [17] is expected to allow the spin-resolved investigation of diffusion dynamics inside the electronic states. Despite considerable efforts to advance SP-STLS techniques [17–20], nanoscopic measurements of diffusive spin dynamics have not yet been realized.

In this paper, we present a technique for visualizing the dynamical footprint of the spin current depending on the spin injection positions using atomic-scale spin injection and circular polarization-resolved photon spectroscopy based on SP-STLS. The atomic-scale accessibility reveals the local electronic states responsible for spin-current scattering, providing insights into the underlying dynamics of the spin current at the local electronic states.

We performed experiments using a low-temperature scanning tunneling microscope (Scienta Omicron, LT STM) operating at 4.6 K under an ultra-high vacuum (UHV) environment. A magnetic field of ±0.2 T was applied in a direction perpendicular to the sample surface using permanent magnets. The field strength was estimated using a Hall probe gaussmeter at room temperature, with the positive direction defined as the direction from the sample to the tip. An iron (Fe) tip was prepared by electrochemically etching an Fe wire (99.5%). The samples were direct bandgap semiconductor *p*-type gallium arsenide (*p*-GaAs), which was heavily doped with zinc (Zn) (2×10^{19} /cm^3). An optical lens (f-number: 1.67, diameter: 11 mm) was installed in the vicinity of the STM stage to collect optical responses, and photons emitted from the sample were guided outside the vacuum chamber for detection. The photon detector was a cooled CCD (Princeton, Spec-10-100B-eX) connected to a spectrometer (Acton, SpectraPro 2300i).

The study of the spin current by SP-STLS in *p*-GaAs depends on the bandgap luminescence. Because spin information is transferred to photon polarization in the luminescence process (Fig. 1a), precise measurements of the energy and circular polarization of the emitted photons can reveal the energy and spin polarization of the electrons responsible for luminescence. The energy and spin polarization correspond to the information after the dynamical processes (Fig. 1a, II), providing quantitative data on the spin-current dynamics in *p*-GaAs. The photon energy (E_{ph}) and circular polarization (P_{ph}) were determined using a spectrometer, a quarter-wave plate, and a linear polarizer (Fig. 1b; see Supplemental Material for details [21]). When a ferromagnetic Fe tip was used to inject spin-polarized electrons into *p*-GaAs with a bias voltage (V_{bias}) of 1.60 V, both clockwise (σ^+) and anticlockwise (σ^-) circularly polarized photons were detected (Fig. 1c). The spectral shape (in this case, the maximum E_{ph} was 1.51 eV) originated from the bandgap luminescence of *p*-GaAs [11], corresponding to the optical transition from the conduction band minimum to the near Fermi level. Although it has been reported that the STM tip itself can also emit circularly polarized photons, this effect becomes negligible when electrons are mainly injected into the conduction band at a sufficiently high V_{bias} (i.e., > 1.6 V) [20]. Moreover, the polarity $\sigma^{+}>\sigma^{-}$ (defined as $P_{ph}>0$) was consistent with the selection rule for *p*-GaAs in the case of the spin-down injection (Fig. 1c, inset) [3,31,32] and switched upon reversing the injected-spin polarity (Fig. 1d). Thus, *p*-GaAs generated circularly polarized photons in response to the spin injection, allowing electron spin to be determined by measuring the photon polarization. Based on the expression $P_{ph}=(\sigma^{+}-\sigma^{-})/(\sigma^{+}+\sigma^{-})$, P_{ph} was estimated to be 15.3%. To convert P_{ph} to electron spin polarization (P_e), the following processes were considered: the optical transition in *p*-GaAs (Fig. 1c, inset), refraction at the *p*-GaAs/vacuum interface [19], and photon detection (see Supplemental Material for detailed estimates [21]). After accounting for these processes, the conversion rate $P_{ph}/|P_e|$ was estimated to be 0.458±0.009, with $|P_e|$=33.4±0.6% at the conduction band minimum. This value corresponds to the spin polarization remaining after spin-current relaxation in *p*-GaAs (Fig. 1a, P_e).

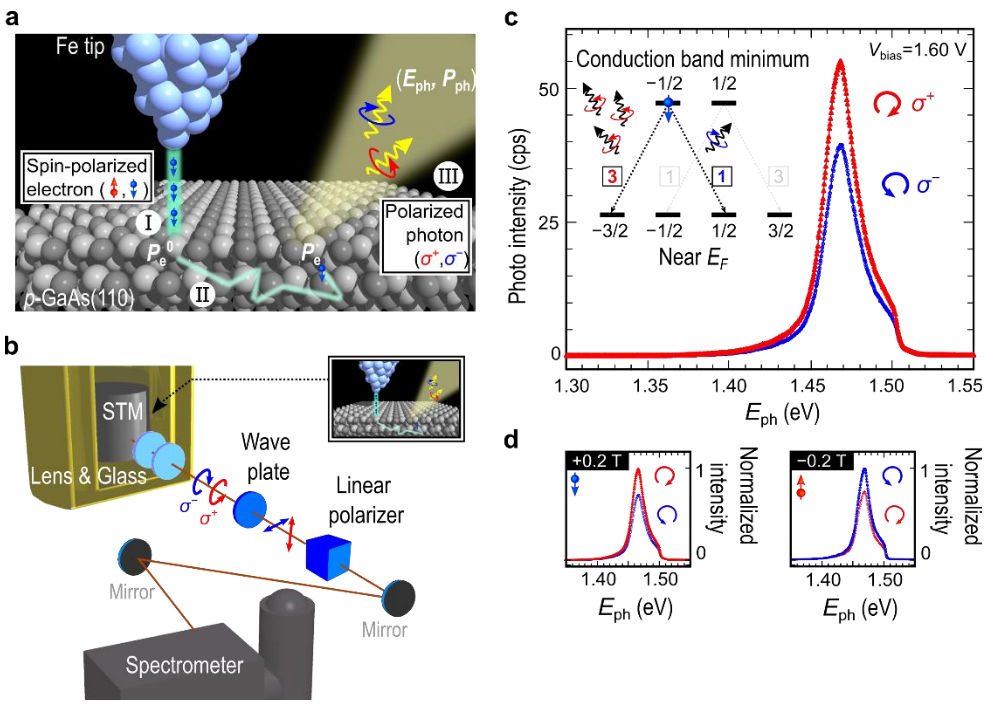

FIG. 1 Spin injection and photon detection by spin-polarized scanning tunneling luminescence spectroscopy (SP-STLS). (a) Experimental setup showing three key processes in SP-STLS: tunneling (I), relaxation (II), and luminescence (III). Fe, iron; *p*-GaAs, *p*-type gallium arsenide; P_e^0 (P_e), initial (final) spin polarization of electrons in *p*-GaAs; P_{ph}, circular polarization of luminescence; E_{ph}, photon energy; σ^+ (σ^-), clockwise (anticlockwise) circularly polarized light. (b) Schematic of an optical system for measuring P_{ph} and E_{ph}. (c) Spectroscopy of σ^+ and σ^- photons (setpoint: 1.60 V, 150 pA). The inset shows the optical transitions (dotted arrows) between the electronic states of *p*-GaAs (black bars), which is known to occur in the ratio 3:1 [3,31,32]. The numbers shown above or below each electronic state indicate their angular momentum. V_{bias}, bias voltage; E_F, Fermi level of *p*-GaAs; cps, counts per second. (d) Magnetic field dependence of normalized luminescence spectra (setpoint: 1.60 V, 150 pA).

Atomic-scale positional control over the site of injection provides the electronic-state selectivity of the spin injection, allowing investigation of the spin-current relaxation at atomic-scale scatterers by monitoring the P_{ph} response (which in this case equals $-0.458P_e$). An atomic-scale map of P_e contrast and STM topography at 1.60 V are shown in Fig. 2a, revealing that P_e in the Ga atomic row (Ga_r) is approximately 40% lower than that in the As atomic row (As_r). This implies that the electron spins injected at Ga_r and As_r underwent different spin dynamical processes. Note that the states of the surface band in III-V semiconductors are localized near the cationic centers on the (110) surfaces (i.e., Ga centers in GaAs(110), Fig. 2b) [11,33]. The P_e contrast therefore indicated that the spin relaxation occurred more strongly in the surface band than in the bulk band because the initial spin polarization (P_e^0) was almost identical in each band (see Supplemental Material for details [21]). SP-STLS thus enabled visualization of the differences in the spin-current relaxation between the individual electronic states via atomic-scale P_e mapping, revealing that the spin relaxation was stronger in the surface band than in the bulk band.

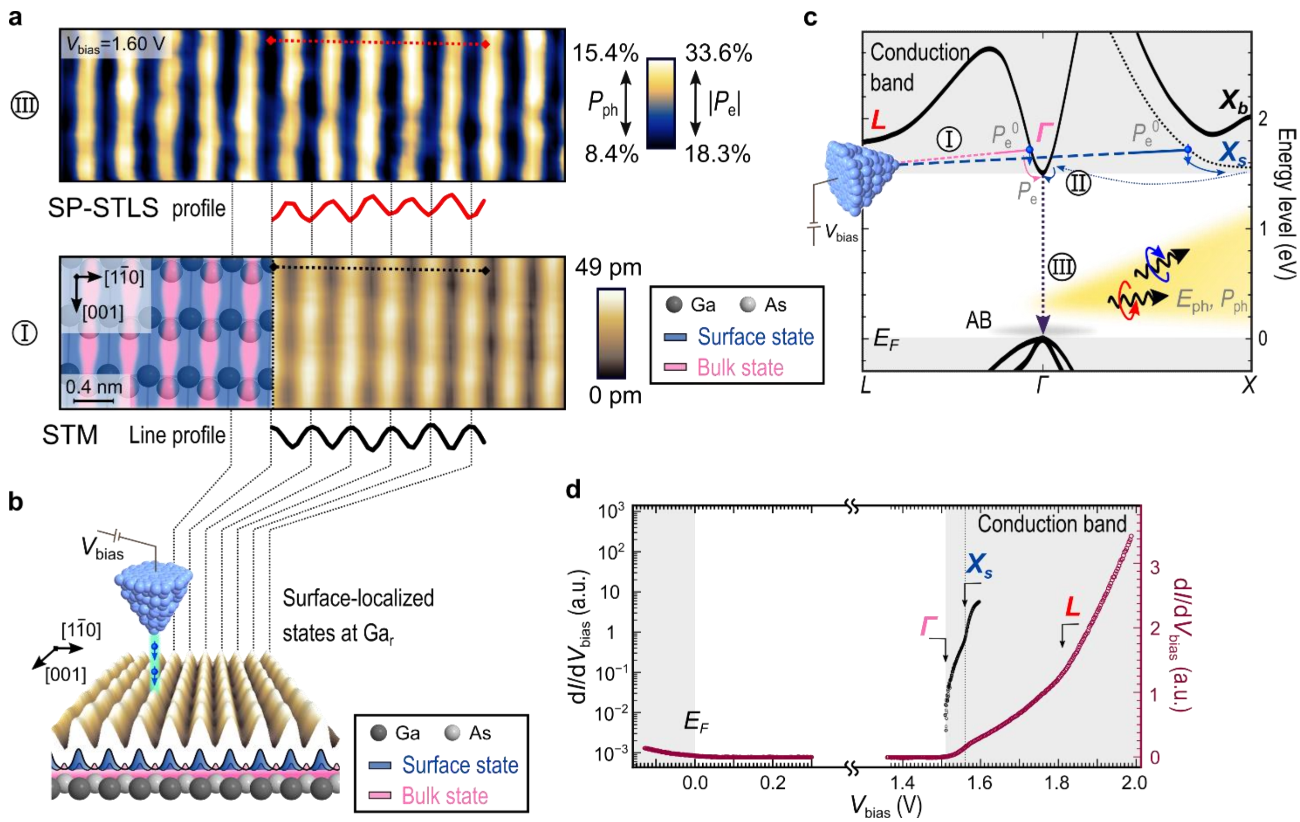

FIG. 2 Atomic-scale SP-STLS mapping reveals spin-current relaxation. (a) Atomic-scale P_{ph} mapping in response to the spin-down injection (top) with an STM topography and the schematic of the atomic structure [11] (bottom). The $|P_e|$ values were estimated using P_e=$-P_{ph}$/0.458 to determine the remaining spin polarization in the conduction band minimum. (setpoint: 1.6 V, 150 pA). (b) Three-dimensional topography of *p*-GaAs with schematic spatial distributions of the densities of states for individual electronic states (blue and pink). Ga_r, gallium atomic row (setpoint: 1.60 V, 150 pA). (c) Band structure of *p*-GaAs showing three valleys of bulk states (Γ, L, and X_b), one valley of a surface state (X_s), and the corresponding possible spin relaxation pathways. AB, acceptor band. (d) Tunnel conductance (dI/dV_{bias}) spectra around the bandgap of *p*-GaAs. Red spectrum was spatially averaged in the surface and black spectrum was taken at Ga_r, in which the individual spectra were taken in different tip conditions. Arrows indicate the valley edges. Setpoints: 1.60 V, 10 pA for red spectrum; 1.60 V, 150 pA for black spectrum; lock-in: 731 Hz, 20 mV for red

spectrum; 817 Hz, 10 mV for black spectrum.

The origin of spin-current relaxation can be associated with the details of the band structure. At the *p*-GaAs(110) surface, the conduction band has three valleys (Γ, L, and X_b) originating from the bulk state and one (X_s) from the surface state (Fig. 2c) [33,34]. Tunnel conductance (dI/dV_{bias}) measurements were performed to determine the energy levels of these valleys (Fig. 2d). The spectra showed a sharp rise at 1.51 V from the Fermi level (0 V), which corresponds to the conduction band minimum (Γ valley edge [34,35]). There were also slight kinks at 1.56 V and at approximately 1.8 V in the dI/dV_{bias} spectra corresponding to the changes in the spatial distribution of dI/dV_{bias} (Fig. S2a [21]). The features were derived from the X_s and L valley edges, respectively, as demonstrated by a dI/dV_{bias} simulation using the effective masses of these valleys (see Supplemental Material for details [21]). Thus, the dI/dV_{bias} measurements at the *p*-GaAs(110) surface revealed that electrons were injected into the individual valleys based on V_{bias}. When V_{bias}=1.60 V (see Fig. 2a), electrons can be injected into both the Γ and X_s valleys but not into the L and X_b valleys. This implies that the atomic-scale P_e mapping measured at 1.60 V (Fig. 2a) visualized the difference in the spin relaxation strength between the Γ and X_s valleys. According to the previous first-principles calculations of the GaAs band structures, the X_s valley showed stronger spin-orbit coupling than the Γ valley owing to the contribution of *p*-like orbitals [33,36], which can cause faster spin relaxation [31]. The spin relaxation difference between the bulk and surface states can therefore be derived from the strength of the spin-orbit coupling in the Γ and X_s valleys, and the stronger spin-orbit coupling in the X_s valley results in a lower P_e at Ga_r in Fig. 2a. Thus, SP-STLS together with the dI/dV_{bias} measurements provided experimental evidence for determining the origin of the spin-current relaxation at the local electronic state, suggesting stronger spin relaxation in the X_s valley owing to the stronger spin-orbit coupling.

Precise control of the V_{bias} plays a key role in the valley-selective spin injection of the SP-STLS, providing insights into the contribution of individual valleys to spin-current relaxation. Figure 3a shows the bias dependence of P_{e} at different tip positions along the $[1\bar{1}0]$ direction. For a lower V_{bias}, P_{e} at $\mathrm{Ga_r}$ exhibited a lower polarization than at $\mathrm{As_r}$ because of the stronger spin relaxation in the X_s valley, as also observed during the P_{e} mapping in Fig. 2a. Interestingly, the local difference in P_{e} gradually vanished at a higher V_{bias} due to an increase in P_{e} at $\mathrm{Ga_r}$, which was clearly observed in the P_{e} plots averaged over $\mathrm{Ga_r}$ or $\mathrm{As_r}$ (Fig. 3b). This indicates that the spin relaxation in the X_{s} valley did not contribute to P_{e} at a higher V_{bias}. Previous experiments have reported that the tunneling probability into the X_s valley [11] decreases with an increase in V_{bias}, which can reduce the electron population in the X_{s} valley at a higher V_{bias}. Therefore, the contribution of the X_{s} valley to P_{e} decreases as V_{bias} increases, revealing that the spin-current relaxation at the surface state is negligible at a higher V_{bias}. When V_{bias} exceeded 1.8 V approximately, P_{e} at $\mathrm{As_r}$ started to decrease monotonically. This implies that the electron spins were injected into the L valley, in addition to the Γ valley, and underwent stronger spin relaxation in the L valley. Previous studies have reported that the spin relaxation is orders of magnitude faster in the L valley than in the Γ valley [35]. Considering this together with the higher tunneling probability into the L valley at a higher V_{bias} (see Supplemental Material for details [21]), the decrease in the P_{e} spectra over 1.8 V was derived from the spin relaxation in the L valley. Thus, the SP-STLS data revealed that the individual valleys affected the spin-current relaxation via tunneling, which in turn enabled bias control of the spin polarization transfer.

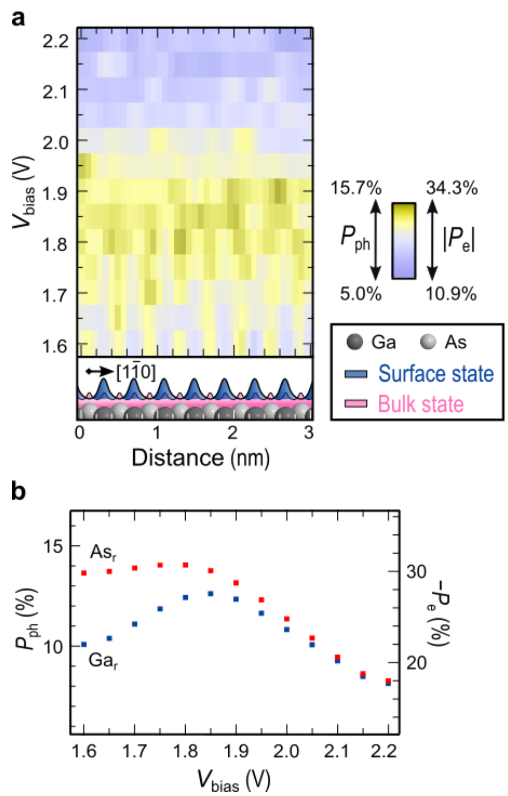

FIG. 3 Bias control of the spin-current relaxation. (a) Bias dependence of the P_e mapping taken along the [1$\bar{1}$0] direction in response to the spin-down injection (top) with schematics of the atomic structure (bottom). Corresponding STM topography is in Fig. 2a (setpoint: 150 pA). (b) Bias dependence of P_e averaged in Ga_r (blue) or in the arsenic atomic row (As_r, red) (setpoint: 150 pA).

An atomic-scale investigation of the spin-current relaxation was achieved by combining a precise spin injection with the spectroscopic detection of photon polarization based on SP-STLS. This study visualized the spin relaxation strength depending on the spin injection positions, revealing the atomic-scale scatterer of the spin current at the *p*-GaAs(110) surface. Precise adjustment of the bias voltage determined the electronic states involved in the spin-current relaxation, providing insights into the origin of spin relaxation based on the band structure. Thus, SP-STLS allows the characterization of the spin-current dynamics beyond the spatial averaging of the local scattering phenomena, thereby presenting a platform for visualizing and controlling the spin current at an atomic scale in the future.

References

[1] Y. K. Kato, R. C. Myers, A. C. Gossard, and D. D. Awschalom, Observation of the spin Hall effect in semiconductors, Science **306**, 1910 (2004). 10.1126/science.1105514

[2] S. Crooker S. A. *et al.*, Imaging spin transport in lateral ferromagnet/semiconductor structures, Science **309**, 2191 (2005). 10.1126/science.1116865

[3] S. Maekawa, *Concepts in Spin Electronics* (Oxford University Press on Demand, New York, 2006).

[4] A. Soumyanarayanan, N. Reyren, A. Fert, and C. Panagopoulos, Emergent phenomena induced by spin–orbit coupling at surfaces and interfaces, Nature **539**, 509 (2016). 10.1038/nature19820

[5] R. Wiesendanger, H.-J. Güntherodt, G. Güntherodt, R. J. Gambino, and R. Ruf, Observation of vacuum tunneling of spin-polarized electrons with the scanning tunneling microscope, Phys. Rev. Lett. **65**, 247 (1990). 10.1103/PhysRevLett.65.247

[6] W. Wulfhekel and J. Kirschner, Spin-polarized scanning tunneling microscopy on ferromagnets, Appl. Phys. Lett. **75**, 1944 (1999). [10.1063/1.124879](10.1063/1.124879)

[7] S. Loth, M. Etzkorn, C. P. Lutz, D. M. Eigler, and A. J. Heinrich, Measurement of fast electron spin relaxation times with atomic resolution, Science **329**, 1628 (2010). 10.1126/science.1191688

[8] A. A. Khajetoorians *et al.*, Current-driven spin dynamics of artificially constructed quantum magnets, Science **339**, 55 (2013). 10.1126/science.1228519

[9] K. Yang *et al.*, Coherent spin manipulation of individual atoms on a surface, Science **366**, 509 (2019). 10.1126/science.aay6779

[10] R. Berndt, J. R. Gimzewski, and P. Johansson, Electromagnetic interactions of metallic objects in nanometer proximity, Phys. Rev. Lett. **71**, 3493 (1993). 10.1103/PhysRevLett.71.3493

[11] H. Imada *et al.*, Atomic-scale luminescence measurement and theoretical analysis unveiling electron energy dissipation at a p-type GaAs (110) surface, Nanotechnology, **26**, 365402 (2015). [10.1088/0957-4484/26/36/365402](10.1088/0957-4484/26/36/365402)

[12] S. W. Wu, N. Ogawa, and W. Ho, Atomic-scale coupling of photons to single-molecule junctions, Science **312**, 1362 (2006). 10.1126/science.1124881

[13] P. Merino, C. Große, A. Rosławska, K. Kuhnke, and K. Kern, Exciton dynamics of C 60-based single-photon emitters explored by Hanbury Brown–Twiss scanning tunnelling microscopy, Nat. Commun. **6**, 8461 (2015). 10.1038/ncomms9461

[14] H. Imada *et al.*, Real-space investigation of energy transfer in heterogeneous molecular dimers, Nature **538**, 7625 (2016). 10.1038/nature19765

[15] A. Stróżecka *et al.*, Electroluminescence of copper-nitride nanocrystals, Phys. Rev. B **90**, 195420 (2014). 10.1103/PhysRevB.90.195420

[16] R. J. P. Román *et al.*, Tunneling-current-induced local excitonic luminescence in p-doped WSe 2 monolayers, Nanoscale **12**, 13460 (2020). 10.1039/D0NR03400B

[17] S. F. Alvarado and P. Renaud, Observation of spin-polarized-electron tunneling from a ferromagnet into GaAs, Phys. Rev. Lett. **68**, 1387 (1992). 10.1103/PhysRevLett.68.1387

[18] V. P. LaBella *et al.*, Spatially resolved spin-injection probability for gallium arsenide, Science **292**, 1518 (2001). 10.1126/science.292.5521.1518

[19] W. F. Egelhoff *et al.*, Spin polarization of injected electrons, Science **296**, 1195 (2002). 10.1126/science.296.5571.1195a

[20] S. Mühlenberend, M. Gruyters, and R. Berndt, Plasmon-mediated circularly polarized luminescence of GaAs in a scanning tunneling microscope, Appl. Phys. Lett. **107**, 241110 (2015). 10.1063/1.4938167

[21] See Supplemental Material at http://link.aps.org/supplemental/***/PhysRevLett.*** for further details on the experimental setup, the photon polarization detection efficiency, the identification of valley edges, the P_e^0 behavior on nonmagnetic materials, the P_e^0 estimation for Fe tip, the master equation analysis, and the estimation of τ_{sX}^{-1}, which includes Refs. [22-30].

[22] D. D. Sell, H. C. Casey Jr, and K. W. Wecht, Concentration dependence of the refractive index for n- and p-type GaAs between 1.2 and 1.8 eV, J. Appl. Phys. **45**, 2650 (1974). 10.1063/1.1663645

[23] B. Engels *et al.*, Comparison between ab initio theory and scanning tunneling microscopy for (110) surfaces of III-V semiconductors, Phys. Rev. B **58**, 7799 (1998). 10.1103/PhysRevB.58.7799

[24] G. J. De Raad, D. M. Bruls, P. M. Koenraad, and J. H. Wolter, Interplay between tip-induced band bending and voltage-dependent surface corrugation on GaAs (110) surfaces, Phys. Rev. B **66**, 195306 (2002). 10.1103/PhysRevB.66.195306

[25] W. Sacks, S. Gauthier, S. Rousset, J. Klein, and M. A. Esrick, Surface topography in scanning tunneling microscopy: A free-electron model, Phys. Rev. B Condens. Matter **36**, 961 (1987). 10.1103/physrevb.36.961

[26] R. Wiesendanger, Spin mapping at the nanoscale and atomic scale, Rev. Mod. Phys. **81**, 1495 (2009). 10.1103/RevModPhys.81.1495

[27] G. Fishman and G. Lampel, Spin relaxation of photoelectrons in *p*-type gallium arsenide, Phys. Rev. B **16**, 820 (1977). 10.1103/PhysRevB.16.820

[28] R. C. Miller, D. A. Kleinman, W. A. Nordland, Jr., and R. A. Logan, Electron spin relaxation and photoluminescence of Zn-doped GaAs, Phys. Rev. B **23**, 4399 (1981). 10.1103/PhysRevB.23.4399

[29] R. J. Soulen *et al.*, Measuring the spin polarization of a metal with a superconducting point contact, Science **282**, 85 (1998). 10.1126/science.282.5386.85

[30] S. K. Khamari, P. Mudi, S. Porwal, and T. K. Sharma, Detection of Optically Injected Spin Polarized Electrons in the L-Valley of AlGaAs through Polarization Resolved Photoluminescence Excitation Spectroscopy, J. Lumin. **213**, 204 (2019). 10.1016/j.jlumin.2019.05.036

[31] M. W. Wu, J. H. Jiang, and M. Q. Weng, Spin dynamics in semiconductors, Phys. Rep. **493**, 61 (2010). 10.1016/j.physrep.2010.04.002

[32] M. I. Miah, Two-photon spin-polarization spectroscopy in silicon-doped GaAs, J. Phys. Chem. B **113**, 6800 (2009). 10.1021/jp900456d

[33] J. L. A. Alves, J. Hebenstreit, and M. Scheffler, Calculated atomic structures and electronic properties of GaP, InP, GaAs, and InAs (110) surfaces, Phys. Rev. B Condens. Matter **44**, 6188 (1991). 10.1103/physrevb.44.6188

[34] J. W. Luo, G. Bester, an A. Zunger, Full-zone spin splitting for electrons and holes in bulk GaAs and GaSb, Phys. Rev. Lett. **102**, 056405 (2009). 10.1103/PhysRevLett.102.056405

[35] T. T. Zhang *et al.*, L-valley electron spin dynamics in GaAs, Phys. Rev. B **87**, 041201(R) (2013). 10.1103/PhysRevB.87.041201

[36] B. K. Agrawal, S. Agrawal, and P. Srivastava, Electronic localized and resonance states of relaxed GaAs (110) surface - An ab initio LMTO approach, Surf. Sci. **408**, 275 (1998). 10.1016/S0039-6028(98)00253-2

Acknowledgments

We thank S. Maekawa, T. Hanaguri, K. Fukutani, N. Hayazawa, and E. Kazuma for the discussions. S. Y. designed and conducted the experiments and performed the analyses; S.Y., H.I., and Y.K. interpreted the results and wrote the manuscript; and Y.K. supervised the project. The present work was supported by the RIKEN postdoctoral research (SPDR) program, MEXT KAKENHI (Grant Nos. 17K18766 and 18H05257), and JST PRESTO (Grant No. JPMJPR1862).